Title

DNA scaffolds enable efficient and tunable functionalization of biomaterials for immune cell modulation

Journal

Nature Nanotechnology, 16(2)

ISSN

1748-3387

Authors

Huang, Xiao
Williams, Jasper Z
Chang, Ryan
et al.

Publication Date

2021-02-01

DOI

10.1038/s41565-020-00813-z

Peer reviewed

HHS Public Access

Author manuscript

Nat Nanotechnol. Author manuscript; available in PMC 2021 June 14.

Published in final edited form as:

Nat Nanotechnol. 2021 February ; 16(2): 214–223. doi:10.1038/s41565-020-00813-z.

DNA scaffolds enable efficient and tunable functionalization of biomaterials for immune cell modulation

Xiao Huang[1,2], **Jasper Z. Williams**[2,3], **Ryan Chang**[1], **Zhongbo Li**[1], **Cassandra E. Burnett**[4], **Rogelio Hernandez-Lopez**[2,3], **Initha Setiady**[1], **Eric Gai**[1], **David M. Patterson**[5], **Wei Yu**[2,3], **Kole T. Roybal**[2,4], **Wendell A. Lim**[2,3,*], **Tejal A. Desai**[1,2,*]

[1]Department of Bioengineering and Therapeutic Sciences, University of California, San Francisco, San Francisco, California, USA

[2]Cell Design Institute and Center for Synthetic Immunology, University of California, San Francisco, San Francisco, California, USA

[3]Department of Cellular and Molecular Pharmacology, University of California, San Francisco, San Francisco, California, USA

[4]Department of Microbiology and Immunology, University of California, San Francisco, San Francisco, California, USA

[5]Department of Pharmaceutical Chemistry, University of California, San Francisco, San Francisco, California, USA

Abstract

Biomaterials can improve the safety and presentation of therapeutic agents for effective immunotherapy, and a high level of control over surface functionalization is essential for immune cell modulation. Here, we developed biocompatible immune cell engaging particles (ICEp) that use synthetic short DNA as scaffolds for efficient and tunable protein loading. To improve the safety of chimeric antigen receptor (CAR) T cell therapies, micron-sized ICEp were injected intratumorally to present a priming signal for systemically administered AND-gate CAR-T cells.

*Correspondence: tejal.desai@ucsf.edu or wendell.lim@ucsf.edu.

Author contributions

X.H., J.Z.W., R.C., K.T.R., W.A.L., and T.A.D. designed the experiments and interpreted the results. X.H., J.Z.W., R.C., Z.L., C.E.B., R.H., I.S., E.G., and W.Y. performed the experiments, and D.M.P. contributed to material designs and synthesis. X.H. analyzed the data and drafted the manuscript. X.H., J.Z.W., R.C., I.S., W.A.L., and T.A.D. edited the manuscript.

Competing interests

T.A.D., W.A.L., X.H., J.Z.W., and R.C. are inventors of pending patents related to the technology described in the manuscript. Z.L., C.E.B., R.H., I.S., E.G., D.M.P., W.Y., K.T.R. declare no competing interests.

Online content

Any methods, Nature Research reporting summaries, source data, supplementary information, acknowledgements, peer review information; details of author contributions and competing interests; and statements of data availability are available in the online version of the paper.

Data availability

The original data of the gel electrophoresis images are publicly available at Dryad Digital Repository (https://doi.org/10.7272/Q6CC0XXJ). Any other raw data that support the plots within this paper are available from the authors upon reasonable request.

Additional information

Supplementary information is available in the online version of the paper. Reprints and permission information is available online at www.nature.com/reprints. Correspondence and requests for materials should be addressed to T.A.D. or W.A.L.

Locally retained ICEp presenting a high density of priming antigens activated CAR-T cells, driving local tumor clearance while sparing uninjected tumors in immunodeficient mice. The ratiometric control of costimulatory ligands (anti-CD3 and anti-CD28 antibodies) and the surface presentation of a cytokine (IL-2) on ICEp were shown to significantly impact human primary T cell activation phenotypes. This modular and versatile biomaterial functionalization platform can provide new opportunities for immunotherapies.

Immune cell therapies have shown great potential for cancer treatment, but still face major challenges of efficacy and safety for therapeutic applications[1–3], for example, chimeric antigen receptor (CAR) T cell treatment[4] for broad patients and solid tumors[5–9]. Immunomodulatory signals including costimulatory ligands[10], cytokines[11–13] and checkpoint inhibitors[14] have been used extensively to boost immune cell activity and modulate tumor environment for improved efficacy[1,3]. Synthetic biocompatible materials have been employed as carriers for these biomolecules to facilitate specific localization and prolonged stability *in vivo* for the modulation of natural or engineered immune cell activities[15–19].

To increase tumor-targeting specificity and avoid “on-target, off-tumor” toxicity in bystander healthy tissues, CAR T cells have been engineered with combinatorial antigen AND-gate activation control that requires sensing two antigens on a target cell, a priming antigen to activate CAR expression and a second antigen to initiate target killing[20,21]. The clinical application of this approach, however, requires knowledge about factors that control T cell activity, such as the tumor-associated antigen density of the AND-gate priming or CAR-targeting antigens[2]. An understanding of the density dependence of antigen-modulated T cell activation is important for therapeutic optimization. Biomaterials presenting the priming signal (natural or synthetic antigen) at a desired density for localized activation of such engineered T cells would mitigate the safety concerns of the dual antigen design[2,21] for translational use. Additionally, synthetic materials with multivalent and multimodal biofunctionalization could advance the needs of cell modulation in immunotherapies[22–26]. Antibody-antigen binding on surfaces requires a certain spatial threshold based on the spatial tolerance of the specific antibody[27], and therefore, a high and controllable density of surface biomolecules could allow for precise control of ligand binding and cell modulation.

Currently, there is an unmet need for robust and biocompatible conjugation strategies to surface-functionalize biodegradable materials with biomolecules (particularly proteins/antibodies) at high densities and to present multiple moieties at precisely controlled ratios[28–30]. PEG (polyethylene glycol) is commonly used as a linker or scaffold for bioconjugation[29], but this method is limited by inefficient presentation of functional groups due to PEG’s flexibility[31]. The surface functionalization of multiple biomolecules and their ratiometric control mostly rely on streptavidin-based chemistry[32] or orthogonal conjugation strategies[33] that can be significantly affected by the chemical properties of the specific cargos. Oligonucleotides have been used as building blocks for origami structures with a controlled display of proteins[34,35] and as surface scaffolds on metallic particles for siRNA delivery[31,36,37], but have yet to be fully utilized for modular and multimodal protein assembly on biodegradable materials[38]. Synthetic short oligonucleotides - natural polymers

with a controllable sequence and unique assembly through Watson-Crick base pairing[35,39] - would be ideal mediators for controlled surface functionalization of biomolecules.

Here, we developed short synthetic DNA scaffolds for the functionalization of biomolecules on the surface of biodegradable particles to extend the immunomodulatory potential (Fig. 1a). For our demonstration platform, we fabricated micron-sized immune cell engaging particles (ICEp) using a biocompatible poly(lactic-co-glycolic acid) (PLGA) polymer[40]. DNA strands were immobilized on the surface of polymeric particles through the emulsion protocol to create an adaptable scaffold for loading bioactive molecules (Supplementary Fig. 1a). Polymer-DNA amphiphilic molecules were synthesized with optimizations including the choice of the polymer, DNA length, solvent, and reaction conditions to form stable PLGA particles with dense DNA scaffolds (Supplementary Fig. 1b–f). The direct incorporation of the reaction mixtures with increasing yield of polymer-DNA conjugate (from varying ratios of thiol-modified DNA to PLGA10k-PEG5k-maleimide) into the emulsion protocol yielded a continuous increase of surface payload-attachable DNA scaffold density (Fig. 1b,c and Supplementary Fig. 1d). Strikingly, the highest average surface loading density on particles (~5 million DNA duplexes per particle, Supplementary Fig. 1g–i) was roughly analogous to the theoretical limit (at ~4 million by footprint calculation, based on ~2 nm diameter of DNA duplex) of a spherical particle with a 2 μm diameter. In particular, this hybridization-guided loading was about 27-fold more efficient than loading from a traditional method[41], in which surface-exposed maleimide groups after particle fabrication using an equal amount of PLGA10k-PEG5k-maleimide were reacted with thiol-modified DNA molecules (Fig. 1b,c). This hybridization-guided assembly protocol is biocompatible, convenient, and rapid such that incubation at room temperature for 2 minutes achieved ~87% of the maximum loading (Fig. 1d and Supplementary Fig. 1j–l).

Furthermore, using unique DNA nucleotide sequences enables independent control of loading multiple cargos on the same material surface (Fig. 1e). Polymer-DNA conjugates with three distinct DNA sequences (namely R, G, and B strands, Supplementary Fig. 2a) were incorporated into the particle emulsion with reaction mixtures at different ratios (3:1:1, 1:1:1, and 1:1:3). After the strands were surface hybridized with a mixture of their respective dye-labeled complementary strands (Fig. 1e), we observed that the ratios of hybridized DNA scaffolds of different sequences on PLGA microparticles were consistent with the polymer-DNA conjugate input (Fig. 1f–h). The ratio of hybridized duplexes is determined by the ratio of surface DNA scaffolds of specific sequence and is rarely affected by the ratio of complementary strands (Supplementary Fig. 2b). In contrast, ratiometric control of such dye-labeled DNA strands on particles using a canonical streptavidin-based method (Supplementary Fig. 2c) was not successful (Supplementary Fig. 2d), which may be affected by the chemical properties of the cargo.

The biocompatibility and biodegradability of the core polymer make this strategy well-suited for *in vivo* applications, and the degradation profile can be easily tuned through the choice of polymer[40]. For example, DNA-scaffolded microparticles can be fabricated using the more stable polymer poly-lactic acid (PLA) and achieve ratiometric control of DNA scaffolds (Supplementary Fig. 2e–j). To accommodate diverse applications, from intracellular payload delivery to extracellular signal transduction, DNA-scaffolded particles

can be synthesized at various sizes and loaded with biomolecules in their core. Particle size can be controlled by tuning key emulsion parameters (Supplementary Fig. 2k,l). Additionally, the core of these particles can be loaded with biomolecules, including oligonucleotides and peptides, through a double-emulsion protocol (Supplementary Fig. 2m–o).

Highly efficient loading of multiple proteins with ratiometric control

Biomolecules can be loaded onto the surface of DNA-scaffolded particles using one of two strategies: a) through a surface step-by-step conjugation via a bifunctional linker; and b) through direct hybridization of complementary DNA-biomolecule conjugates to the scaffold (Fig. 2a). In the case of a fluorescently labeled human IgG, surface step-by-step conjugation saturated protein loading even with increased densities of available DNA linkers on the surface (Fig 2b,2c and Supplementary Fig. 3a). In contrast, the hybridization-guided assembly strategy showed a ~3-fold higher level of IgG loading than the surface conjugation method for particles with denser DNA scaffolds ($P = 0.0002$), and the increase in IgG loading corresponded to the increase in scaffold density (Fig. 2b). The highest level of IgG loading achieved (at ~0.6 million per particle) was again comparable to the theoretical footprint limit of a spherical particle at 2 μm in diameter (~0.64 million per particle, based on ~5 nm diameter of IgG) (Fig. 2b). To generate DNA-antibody conjugates with minimal impact on antibody activity, a “TCEP” strategy[42] was chosen whereby the antibody hinge region was selectively reduced to expose the thiol group to conjugate with a complementary DNA strand. Using this conjugation strategy, anti-PD-L1 antibody, a checkpoint inhibitor, showed intact binding activity (Supplementary Fig. 3b,c), and its loading on PLGA microparticles resulted in high binding specificity for PD-L1-positive cells (Fig. 2c). In addition, increasing levels of anti-PD-L1 loading from varying densities of DNA scaffolds on particles (Fig. 2b, “Low, Medium and High”) correlated to increasing levels of PD-L1 antigen binding (Fig. 2d–f). For DNA tethering of proteins other than antibodies, other conjugation options are available to yield products with intact activity (Supplementary Fig. 3d,e).

Using ratiometrically controlled sequences on PLGA particles (Fig. 1f,g), we co-loaded three proteins (GFP and two antibodies), each individually attached to one of the three unique complementary DNA strands, through hybridization-guided assembly (Fig. 2g). The distribution of each protein cargo correlated to the respective scaffold population (Fig. 2h,i), demonstrating the robust ratiometric control achieved using this strategy. We also tested the ratiometric control of biotinylated proteins (GFP and two antibodies tagged with different fluorescent dyes) on streptavidin-coated particles, but this streptavidin-based strategy showed limited control (Supplementary Fig. 3f).

Compatibility of this platform for *in vivo* applications

To enable *in vivo* use, we explored the stability of the DNA scaffolds on PLGA microparticles in the presence of a large excess of DNase (Fig. 3a). We observed an almost complete (~87%) degradation of DNA scaffolds after DNase treatment; however, this dropped to ~20% with moderate IgG coverage (~1/4 of the highest IgG loading) (Fig. 3b).

This suggests that surface-loaded proteins are able to protect DNA scaffolds through steric hindrance. In human serum, we did not observe as much DNA degradation for the non-scaffolded particles (~29%), which may be due to the comparatively lower levels of DNase in serum than used in Fig. 3a,b; however, the degree of DNA degradation similarly decreased when proteins were attached to the surface (Fig. 3c).

We evaluated the feasibility of using local particle delivery to send spatially defined signals to therapeutic cells *in vivo*. We labeled DNA scaffolds on PLGA microparticles with infrared dye Q705, and we monitored the distribution and half-life of their surface-coating through IVIS near-infrared fluorescence imaging after injecting particles intratumorally in NSG mice with subcutaneous K562 xenograft tumors (Fig. 3d). Microparticles with diameters of ~2 μm were retained locally within the tumor (Fig. 3d and Supplementary Fig. 4a) for more than a week, with a gradient distribution around the injection site (Fig. 3e) and minimal distribution to other organs (Supplementary Fig. 4b,c). Fluorescence quantification of IVIS images and tumor sections showed stable surface loading on particles with a half-life of ~2–4 days (Fig. 3d,f and g), while free dye signal without particle carriers diminished rapidly after 6 hours (Supplementary Fig. 4d,e). These results demonstrate that injections of DNA-scaffolded microparticles can be used to send localized, sustained signals to therapeutic cells *in vivo*.

We then investigated the safety of intravenous injection of DNA-scaffolded particles (carrying ~20 μg isotype IgG) in BALB/c mice by serum cytokine/chemokine quantification (mouse cytokine/chemokine 31-plex) and clinical chemistry analysis of blood collected 2 days later. Treatments with PLGA nanoparticles (~250 nm diameter) and microparticles (~1.5 μm diameter) tethered with DNA scaffolds and mouse isotype IgG both showed similar levels of blood cytokines compared to the PBS treatment control (Supplementary Fig. 4f). The blood clinical chemistry values for micro- and nanoparticles were comparable to the PBS control, all falling within the normal range as referenced from the University of Arizona animal care (Supplementary Fig. 4g).

Since macrophage uptake could be an obstacle[43] for particle-based drug delivery *in vivo*, we incorporated a CD47-mimic “self”-peptide[44] onto DNA-scaffolded PLGA microparticles to reduce possible phagocytosis by macrophages (Supplementary Fig. 4h). Fluorescein-labeled PLGA microparticles with and without the surface-loaded “self”-peptide were co-incubated with a mouse macrophage line J774A.1 *in vitro*. The surface decoration of a “self”-peptide significantly reduced the uptake of these particles by macrophages (Supplementary Fig. 4h,i, $P = 0.0004$). This “self”-peptide functionalization provides a possible strategy to reduce the clearance of particles *in vivo*.

Design of particles to prime activation of AND-gate CAR-T cells

We tethered an orthogonal antigen (GFP) on micron-sized ICEp to prime AND-gate CAR-T cells engineered with antigen recognition circuits, thus restricting CAR-T cytotoxicity to tumors locally injected with microparticles (Fig 4a). These AND-gate T cells utilize a modular synthetic Notch (synNotch) receptor with an extracellular domain to recognize a target antigen and an intracellular transcriptional activator (TF) domain to control the

expression of a CAR targeting a second antigen[20]. Killing is only induced when both antigens are presented to T cells, with one activating the synNotch receptor to release the TF domain for CAR expression and the other activating CAR-mediated cytotoxicity[20]. Herein, human primary T cells were transduced with a gene encoding a constitutively-expressed synNotch receptor with an extracellular anti-GFP nanobody and an intracellular Gal4DBD-VP64 synthetic transcription factor (TF) domain, together with a TF-inducible CAR gene targeting HER2 (human epithelial growth factor receptor 2)[20] (Fig. 4a). In this system, T cells only express anti-HER2 CAR and kill HER2-positive target cells after being primed by the anti-GFP synNotch binding of ICEp-presented GFP.

Human primary CD8+ T cells engineered with the synNotch receptor - CAR circuit were co-cultured for 24 hours with single-antigen target cells (human melanoma cell line A375 with HER2 overexpressed) in the presence or absence of GFP+ ICEp microparticles. SynNotch CAR T cells showed selective expression of the early activation marker CD69 in the presence of both HER2+ A375 cells and GFP+ ICEp, and the activation was similar to T cells exposed to dual-antigen target cells (human leukemia cell line K562 with GFP and HER2 co-expressed) (Supplementary Fig. 5a). Engineered T cells also showed AND-gate killing behavior, selectively killing HER2+ A375 cells in the presence of ICEp microparticles with GFP (Fig. 4b,c and Supplementary Fig. 5b–d). Importantly, we observed density-dependent activation of the synNotch receptor for cytokine release in both CD4+ and CD8+ CAR-T cells (Fig. 4d, and Supplementary Fig. 5e) and target killing by CD8+ cells (Fig. 4e). ICEp presenting a lower density of the GFP antigen may result in inadequate expression of HER2-CAR on T cells for robust activity, explaining why initial attempts using particles functionalized by traditional surface conjugation chemistry and with a far lower GFP density failed to activate synNotch CAR-T cell toxicity (Fig. 4e). Importantly, antigen-presenting ICEp showed significant advantages in the activation of murine immune cell lines compared to antigen-presenting K562 cells (Fig. 4f,g, $P < 0.0001$ for all three), demonstrating the usefulness of this platform for logic-gated cell modulation.

When saturated densities of GFP were loaded on ICEp of different sizes (“Nano”, “Medium” and “Micro”, corresponding to Supplementary Fig. 2l), they activated CD8+ synNotch CAR-T cells and had similar efficiencies of killing to the target HER2+ A375 cells (Supplementary Fig. 5f). The co-incubation of target cells with synNotch CAR-T cells in the absence of ICEp showed moderate cytotoxicity (Fig. 4c and Supplementary Fig. 5b–d,f), which is likely due to the leakiness of inducible CAR expression. This phenomenon was also observed in previous reports and can be improved through further optimization of synNotch receptors.

We hypothesized that GFP-decorated PLGA microparticles could be injected intratumorally as a local activator for systemically administered anti-GFP synNotch/anti-HER2 CAR T cells (Fig. 4h). NSG mice were implanted subcutaneously with the same HER2-overexpressed K562 xenograft tumors in their bilateral flanks as a model for tumor and healthy tissue both expressing the CAR antigen. After a week, mice were intravenously administered synNotch CAR-T cells once in combination with 4 doses of intratumorally injected ICEp (Fig. 4h). The size of ICEp-injected ipsilateral tumors decreased over time, in contrast to the contralateral tumors within the same mice without ICEp injection and tumors

in mice injected with ICEp plus untransduced primary T cells (Fig. 4i and Supplementary Fig. 5g). We also performed fluorescence microscopy on fixed tumor samples of mice sacrificed at an earlier timepoint (day 15) and observed selective T cell enrichment in the ICEp-injected tumor (Fig. 4j,k). These results demonstrate that ICEp can provide spatially controlled signals *in vivo* for the local activation of synNotch CAR-T cells and induction of tumor clearance with a limited risk of cross-reaction against healthy tissues.

Design of optimized particles for natural T cell activation

To demonstrate the versatility of this platform for immune cell modulation, we engineered T cell costimulatory ligands anti-CD3 and anti-CD28 on biodegradable PLGA microparticles, termed anti-CD3/CD28 ICEp, to activate human primary T cells *ex vivo* (Fig. 5a,b and Supplementary Fig. 6a). Starting with the same particle-to-cell ratio as commercial anti-CD3/CD28 Dynabeads, T cells underwent massive expansion with a cell yield that is higher at day 8 and equivalent at day 14, compared to Dynabead-mediated activation across three independent CD4+ and CD8+ T cell donors (Fig. 5c and Supplementary Fig. 6b). To investigate the exhaustion phenotype of expanded CD4+ and CD8+ T cells at day 14, we examined cell exhaustion markers LAG-3, PD-1, and TIM-3 (Supplementary Fig. 6c). With the added benefit of not having to remove degradable ICEp (Supplementary Fig. 6a), we found that the populations of exhaustion marker positive cells among the three donors were consistent and generally lower with ICEp, compared to those activated by Dynabeads (Fig. 5d and Supplementary Fig. 6d). We also reduced the total amount of anti-CD3 and anti-CD28 on ICEp from “Full” to “1/5” (Supplementary Fig. 6e) and found that the impact of lowering antibody density on CD8+ T cell expansion is donor-dependent: two donors showed significantly less cell expansion (D1, $P = 0.0306$; D2, $P = 0.0457$), while three others showed significantly more expansion (D3, $P = 0.0023$; D4, $P = 0.0193$; D5, $P = 0.0457$) (Supplementary Fig. 6f).

Given the ability of this platform to precisely control the ratio of multiple surface proteins, we modulated anti-CD3 and anti-CD28 antibodies on ICEp at ratios ranging from 1:5 to 5:1 to activate human T cells and observed a linear increase of cell yield from ICEp-[1:5] to ICEp-[3:1] for both CD4+ and CD8+ cells at day 14 (Fig. 5e,f). For CD8+ T cells, the exhaustion phenotype (population of 0, 1–3 exhaustion marker expression) was significantly different between ICEp-[1:5] and ICEp-[3:1] mediated activation for 14 days among the three donors (Fig. 5g, $P = 0.0003$). For CD4+ T cells, only the population of non-exhausted cells was significantly different between the two ratios (Supplementary Fig. 6g, $P = 0.0068$). Additionally, the cell differentiation phenotype of T cells on day 7 after ICEp activation was explored by measuring the expression of CD45RA and CCR7 surface markers (Fig. 5h). The cell populations of each gated quadrant between ICEp-[1:5] and ICEp-[3:1] mediated activation were significantly different within a donor (Fig. 5i, CD45RA+CCR7+, $P < 0.0001$; CD45RA-CCR7+, $P = 0.0016$; CD45RA-CCR7-, $P < 0.0001$; CD45RA+CCR7-, $P = 0.0044$). With a flow cytometry panel (CD45RA, CCR7, CD27, CD45RO, CD62L and CD95) analysis[45] (the same donor), we observed a dramatically different pattern of cell differentiation between ICEp-[1:5] and ICEp-[3:1] mediated activation and identified that the population of CD45RA+CCR7+ cells are also CD45RO+ and are, therefore, central memory (CM) cells (Supplementary Fig. 6h). Among five donors, the cell differentiation

phenotype represented by the expression of CD45RA and CCR7 markers (CD45RA +CCR7+ and CD45RA-CCR7+: central memory, CD45RA-CCR7-: effector memory, CD45RA+CCR7-: terminally differentiated effector memory) showed a dramatic difference between ICEp-[1:5] and ICEp-[3:1] mediated activation as well (Supplementary Fig. 6i, $P < 0.0001$). Overall, we demonstrated that key immune cell properties, from cell expansion to exhaustion and differentiation phenotypes, are impacted by the ratiometric control of anti-CD3 and anti-CD28 on ICEp, thus highlighting potential new opportunities for immune cell modulation.

Interleukin-2 (IL-2) is an important cytokine signaling molecule in the immune system, but its significant systemic toxicity at high doses limits its clinical uses[1]. The surface-presentation of IL-2 on biomaterials may prolong its half-life and minimize its systemic toxicity through local administration[42]. Here, we validated this approach as an alternative to the standard protocol of supplementing free IL-2 in media for *ex vivo* T cell culture[32]. We presented IL-2 on the surface of ICEp via its antibody clone #5355, which was engineered to facilitate the binding of IL-2 to its β and γ receptor on T cells, thus promoting the proliferation of non-Treg T cells[46] (Fig. 5j). Using ICEp-bound IL-2 supplemented in the medium (0.005 OD550 ICEp carrying 0.57 ng/mL IL-2, Supplementary Fig. 6j) after ICEp-anti-CD3/CD28-[3:1] mediated activation, we yielded significantly higher folds of cell expansion (at day 14) than an equivalent amount of free IL-2 supplementation (0.54 ng/mL) for both CD4+ and CD8+ T cells across four independent T cell donors (Fig. 5k,l, $P = 0.0001$ for CD4+ and $P = 0.0024$ for CD8+). Importantly, the higher fold of expansion with ICEp-bound IL-2 supplementation did not lead to a higher level of exhaustion for both CD4+ and CD8+ T cells (Fig. 5m). We observed similar levels of CD4+ and CD8+ cell expansion between the standard protocol with free IL-2 and ~10 folds less ICEp-bound IL-2 (Supplementary Fig. 6k). This can be beneficial for both *ex vivo* T cell expansion and local administration of IL-2 presenting ICEp at the tumor site to activate immune cells *in vivo*.

Conclusions

We demonstrated a unique platform using synthetic short DNA oligonucleotides as surface scaffolds on biodegradable materials for the precise and controlled loading of multiple biomolecules at a specific ratio and density. A series of studies were carried out to achieve the maximum loading density, ratiometric control, adaptability to different particle sizes/composition, and feasibility for *in vivo* use. We demonstrated that: **i**) a range of immune modulators (e.g. antigen, costimulatory ligand, checkpoint inhibitor, cytokine) can be loaded on ICEp with intact bioactivity; **ii**) antigen-presenting ICEp can be administered locally to control AND-gate CAR-T cell activation and tumor clearance *in vivo*; and **iii**) the ratiometric control of costimulatory ligands (anti-CD3 and anti-CD28) and the presentation of IL-2 on ICEp surfaces can influence *ex vivo* T cell activation and expansion. Through this highly modular platform, biocompatible materials can be employed as substrates for a wide spectrum of modulatory biomolecules, including cytokines[47], antigens[48], checkpoint inhibitors[13], agonistic or antagonistic antibodies[49], adjuvants[50,51], etc., to regulate the local environment and enhance the efficacy of immune cells in cancer immunotherapy[52].

Methods

Synthesis of Thiol-modified DNA

3'Thiol-modified DNA was synthesized on 3'thiol-modifier 6 S-S CPG beads (Glen Research #10–1936-02) using an Expedite 8909 DNA synthesizer. DNA oligos were retrieved from the beads by incubation at 70°C for 20 minutes in the presence of AMA solution (Ammonium hydroxide:Methylamine=1:1,v/v), followed by vacuum evaporation (SpeedVac, ThermoFisher #SPD121P-230) for 3 hours to remove AMA. DNA oligos were reconstituted in TE buffer (Tris-EDTA, 10mM, pH7.5), then filtered through a 0.22 μm filter (Millipore #UFC30GV00) and stored at −20°C.

Synthesis of polymer-DNA amphiphilic molecule

3'Thiol-modified DNA oligos were deprotected through treatment with a 100x molar excess of Tris(2-carboxyethyl)phosphine hydrochloride solution (TCEP, Sigma #646547) at 37°C for 1 hour, and purified by size-exclusion chromatography (Glen Research #61–5010). Unless otherwise specified, freshly prepared thiol-DNA 17mer at 200 μM were reacted with poly(lactide-co-glycolide)-b-poly(ethylene glycol)-maleimide (Mw 10,000:5000 Da, PLGA10k-PEG5k-Mal, Akina #AI053) at a 1:1 ratio in a solvent composed of dimethylformamide (DMF)/H_2O (90:10,v/v) and 0.2% triethanolamine and incubated at room temperature overnight. The next day, the solvent was removed by vacuum evaporation at 70°C for 3 hours, and the dried mixture was stored at −20°C. The product was verified by TBE-Urea gel electrophoresis (15%, ThermoFisher #EC68855) with SYBR gold dye staining (ThermoFisher #S11494), and the conjugation efficiency was quantified by gel densitometry analysis using GelQuantNET 1.8 software.

Fabrication of polymeric particles with DNA

To fabricate PLGA particles of varying sizes (Supplementary Fig. 2j), the dried polymer-DNA reaction mixture, (from 100 nmol of each reactant) reconstituted in 200 μL solvent (ethyl acetate:H_2O=1:1,v/v), was incorporated into a mixture containing 0.5 mL ethyl acetate (EtOAc), a certain amount of unmodified polymer (Poly-lactic-co-glycolic acid, 50:50, Mw 38,000–54,000, Sigma #719900), and 0.5 or 1.0 mL aqueous buffer (10mM sodium citrate, 600 mM Na^+, pH3.0) that either included or did not include 1% polyvinyl alcohol (PVA, Sigma #81381). The whole mixture was then vortexed and probe-sonicated (Fisher miniRoto S56) on ice at 7–8 W for 5 × 5 s with 10 s intervals. After sonication, the mixture was immediately combined with 9 mL 0.2% PVA and stirred in a chemical hood for 3 hours so that the ethyl acetate could evaporate. Particles were then filtered through a 40 μm cell strainer (Sigma #CLS431750) and washed through centrifugation at 10,000 x g for 10 minutes. The pellet was then resuspended in TE buffer (10mM Tris-HCl, pH8.0) with 0.01% Tween-20 added. This washing protocol remained the same for later fabrications. After three washes, particles were suspended in TE buffer with 1% PVA and lyophilized (VirTis Advantage Plus) for long term storage. The size profile of particles was characterized by dynamic light scattering (DLS) with a Malvern Nano ZS instrument and SEM imaging using a Zeiss Ultra-55 scanning electron microscope (SEM). The particle concentration was normalized using the optical density at 550 nm (OD550) measured from a UV-Vis spectrometer (Molecular Devices SpectraMax M5).

The same fabrication protocol was used for PLA microparticles, but the emulsion mixture was adjusted: 0.5 mL dichloromethane (DCM) with 100 mg/mL polylactic acid (Mw 60,000, Sigma #38534), 0.5 mL aqueous buffer (10 mM sodium citrate, 600 mM Na^+, 0.3% PVA, pH3.0), and the polymer-DNA reaction, (from 200 nmol of each reactant) reconstituted in 200 μL solvent (ethyl acetate:H_2O=1:1,v/v). To encapsulate biomolecules in the core of DNA-scaffolded particles, another emulsion step was added before the above emulsion: biomolecules, including 0.25 mg FITC-labeled peptide with 21 amino acids (LifeTein) and 50 nmol 5'Cy3-labeled DNA-21mer (Bioresearch Technologies), dissolved in 50 μL PBS (phosphate-buffered saline, pH7.0) was mixed into the 0.5 mL ethyl acetate solution with dissolved PLGA (Sigma #719900), and probe-sonicated at 7–8 W for 5 × 5 s with 10 s intervals on ice. Immediately after this, the amphiphilic polymer-DNA and an aqueous buffer were added following the same protocol described above.

Attachment of complementary DNA to proteins and their purification

IgG antibodies were attached to complementary DNA strands through the "TCEP" strategy. Various modified complementary DNA strands were all from Biosearch Technologies. Antibodies were first exchanged in reducing buffer (PBS with 10 mM EDTA) by size exclusion chromatography (Zeba Spin Desalting Column, ThermoFisher #89882), and the disulfide bond at the hinge region was selectively reduced through the addition of TCEP at a 3 molar or 4.5 molar excess and subsequent incubation at 37°C for 1 hour. Excess TCEP was removed through size exclusion chromatography. 3'-NH2-modified complementary DNA was conjugated to a MAL-dPEG4-NHS linker (Quanta Biodesign #10214) with a 30-fold molar excess in HEPES buffer (pH7.0) at 37°C for 1 hour, followed by the removal of the unconjugated linker through a 70% ethanol precipitation and size exclusion chromatography. The reduced antibody and modified DNA were combined at a 1:10 molar ratio and incubated at 37°C for 1 hour then 4°C overnight. The next day, DNA-protein conjugates were purified using protein G affinity chromatography (Genscript #L00209) to remove unconjugated DNA.

The anti-PD-L1 (Bio X cell #BE0285) antibody was conjugated to 3'NH2–5'Quasar570-modified DNA 22mer through a HyNic-4FB linker (TriLink, #S-9011) following the kit's instructions. As a validation of the antibody activity post-conjugation, purified anti-PD-L1-DNA conjugates from the "TCEP" strategy and the TriLink strategy and PE anti-human PD-L1 (Biolegend #329705, 1:500 dilution) were incubated with PD-L1-overexpressing K562 cells at 4°C for 30 minutes, followed by two washes (centrifugation at 400 x g for 5 minutes and resuspension in PBS) for flow cytometry with a BD LSR II. Anti-PD-L1-DNA conjugates linked through the "TCEP" strategy were loaded onto DNA-scaffolded PLGA microparticles. PD-L1-overexpressed and wildtype K562 cells at 1 million/mL were added to particles at 0.3 OD550 and incubated for 30 minutes at 37°C, followed by cell nuclei staining with Hoechst 33342 (ThermoFisher #62249). Imaging was performed using the spinning disk confocal fluorescence microscope (Nikon Yokogawa CSU-22).

His-tag GFP were expressed by Escherichia coli BL21 (DE3) (Novagen) transduced with pRSET-EmGFP vector (ThermoFisher, #V35320) in E. coli expression medium (MagicMedia, Invitrogen #K6803). His-tag GFP was extracted using cell lysis reagent

(Sigma, #B7435) then purified using nickel-nitrilotriacetic acid affinity chromatography (Invitrogen #R90115). The MAL-PEG4-NHS linker (Quanta Biodesign) was mixed with GFP at a 30-fold molar excess and incubated at 37°C for 1 hour; size-exclusion chromatography was then used to remove the excess linker. 3'Thiol-modified complementary DNA was decapped using the protocol described above and reacted with modified GFP at a 1:10 molar ratio at 37°C for 1 hour then 4°C overnight. The next day, GFP-DNA conjugates were purified using nickel-nitrilotriacetic acid affinity chromatography to remove unconjugated DNA. Protein-DNA conjugates were analyzed through SDS-PAGE gel electrophoresis (Genscript #M42012L) with SYPRO Ruby dye staining (ThermoFisher #S21900).

Ratiometric control of surface DNA scaffolds with different sequences and the co-loading of versatile payloads

3'Thiolated DNA with different sequences were synthesized, namely R, G, and B (Supplementary Fig. 2a). Following the conjugation with PLGA10k-PEG5k-Mal (Akina, #AI053), polymer-DNA molecules from different sequences were mixed at varying ratios and incorporated into the particle fabrication process described above (100 nmol for each reactant). Strands complementary to the DNA scaffolds that were pre-conjugated with small molecules (e.g. fluorescent dye or biotin, at 1 μM/OD550) or proteins (e.g. GFP or antibodies, at 180 nM/OD550) were incubated with particles at 37°C for 30 minutes in PBS buffer with 600 mM Na^+ and 0.01% Tween-20 supplemented for the surface hybridization of payloads. The excess was removed by three washes. For co-loading of multiple cargos, the input proportion of each individual strand with a specific sequence was consistent with its DNA-polymer counterpart input during the particle fabrication. To control GFP density on DNA-scaffolded particles, an excess amount of complementary DNA-GFP conjugates were hybridized to particles with a corresponding scaffold sequence determined at different densities (e.g. 1/3, 1/2 or full in Fig. 4d). Another method of adjusting the density of GFP was the hybridization of full-density DNA-scaffolded particles with complementary DNA-GFP at varying concentrations (e.g. 15 nM/OD, 30 nM/OD, 60 nM/OD and 180 nM/OD in Fig. 4e).

The loading efficiencies of different cargos on the surface or in the core were quantified through a fluorescence-based assay using dye-labeled DNA strands (5'Quasar570-compR, 5'FITC-compG, 5'Quasar705-compG, 5'Quasar670-compB, Supplementary Fig. 2a), peptides (C-terminus FITC-labeled peptide, LifeTein, LLC), or proteins (FITC-labeled human IgG, Sigma #SLBW7799) after etching the particles with dimethyl sulfoxide (DMSO) and diluting with 9x volume of water. The fluorescence signal was detected by a plate reader (Tecan Spark with Tecan SparkControl Software V2.1) and analyzed using a calibration curve normalized from OD550. Functionalized microparticles with fluorescent labels were imaged through a spinning disk confocal fluorescence microscope (Nikon Yokogawa CSU-22 with NIS Elements AR 5.21.00_b1483), and the size distribution was quantified using ImageJ software analysis from acquired images. Fluorescent microparticles were also analyzed the concentration using a cell counter (Countess II FL AMQAF1000, ThermoFisher).

Loading of biotinylated biomolecules on streptavidin-coated microparticles and the ratiometric control

To conjugate streptavidin onto the surface of particles with maleimide functional groups, streptavidin (Prozyme #SA10) was reacted with an SPDP (N-Succinimidyl 3-(2-pyridyldithiol)propionate) linker (Sigma, #P3415) at a 20-fold molar excess in HEPES buffer (pH7.0) at 37°C for 1 hour. The size-exclusion chromatography was then used to remove excess SPDP and exchange to the reducing buffer (PBS with 10 mM EDTA). A 30-fold molar excess of TCEP was then added to reduce streptavidin-SPDP to free thiols. This mixture was incubated at 37°C for 1 hour, then added onto maleimide-presenting particles at 1.0 mg/mL per OD550. The mixture containing streptavidin-SPDP and particles was incubated at 37°C for 1 hour, then the particles were washed three times.

To load biotinylated DNA on streptavidin-coated particles, DNA strands with different fluorescent labels (5'FITC-compG-3'biotin, 5'Quasar705-compG-3'biotin, and 5'Quasar570-compR-3'biotin) were individually added or mixed at certain molar ratios to particles with a total of 180 nM/OD550. The mixture was incubated at room temperature for 30 minutes so that the DNA can bind with streptavidin on the surface of the particles, then the particles were washed three times. Particles were dissolved by DMSO, and the fluorescence signal was analyzed using the plate reader as described above.

For the biotin-modification of proteins, GFP was reacted with a 10x molar excess of NHS-PEG_4-biotin (Quanta Biodesign #10200) in $NaHCO_3$ buffer (10 mM, pH 8.0) for 1 hour at 37°C; IgG antibodies were reduced using the "TCEP strategy" as described above and were reacted with 10 x molar excess of MAL-PEG_3-biotin (Quanta Biodesign #10201) in PBS buffer with 10 mM EDTA for 1 hour at 37°C. The excess biotin was removed through two rounds of purification with size-exclusion chromatography, and then the protein concentration was quantified using a spectrophotometer. The biotinylated antibodies were further fluorescently labeled through a reaction with NHS-AFDye555 (Click Chemistry Tools #1341) or NHS-Cy5 (Lumiprobe #13020) with an 8x molar excess at 37°C for 1 hour. To remove the unconjugated dye, the biotinylated antibodies were then purified twice using size-exclusion chromatography. The protein concentration was also determined by spectrophotometer quantification. Modified proteins (biotin-GFP, biotin-IgG-Cy5, and biotin-IgG-AF555) were added individually or mixed at specific molar ratios to streptavidin-coated particles at 0.1mM total per OD550 with 1% BSA/PBS. After an incubation at room temperature for 30 minutes, the particles were washed twice. Particles were analyzed the fluorescence signal using the plate reader, and the signals were normalized by OD550.

Antigen binding activity of anti-PD-L1 antibody loaded particles

PLGA microparticles assembled with anti-PD-L1 antibodies were added to an excess amount of biotinylated human PD-L1 (4 μg/mL per OD550, Sino Biological #10084-H08H-B or Acro Biosystems #PD1-H82E5) in 1% BSA/PBS. The mixture underwent an incubation at room temperature for 30 minutes, then the particles were washed twice. In a separate reaction, streptavidin was fluorescently labeled with FITC or AFDye555 dye through a reaction with an 8x molar excess of NHS-FITC (ThermoFisher #46409) or NHS-AFDye555 (Click Chemistry Tools #1341) in $NaHCO_3$ buffer (10 mM, pH 8.0) for 30

minutes at 37°C. Afterwards, the fluorescently labeled streptavidin was purified twice via size exclusion chromatography (Glen Research #61–5010) in order to remove the unconjugated dye. A large excess of fluorescently labeled streptavidin (~150 μg/mL per OD550) was added to biotinylated PD-L1-bound particles in 1% BSA/PBS and incubated at room temperature for 30 minutes, and then the particles were washed twice. Particles were imaged using the spinning disk confocal fluorescence microscope (Nikon Yokogawa CSU-22), and images were analyzed using the ImageJ software, which detects the mean fluorescence intensity of particles.

Traditional surface step-by-step conjugation for payload attaching

To attach thiol-modified biomolecules or IgG antibodies onto particles without DNA scaffolds, particles with maleimide functional groups on the surface were fabricated with all of the steps of above protocol, with the replacement of polymer-DNA reaction mixture by 100 nmol PLGA-PEG-MAL (Akina #AI053). Freshly prepared particles with maleimide functional groups were then reacted with either 3'thiol-5'Quasar670-modified DNA at 1 μM/OD550 or reduced antibodies with free thiols (FITC-IgG, Sigma) at 180 nM/OD550 for 1 hour at 37°C then 4°C overnight. The next day, particles were washed and quantified through the fluorescence-based analysis.

To conjugate IgG molecules onto the surface of particles using DNA scaffolds, particles were first hybridized with 3'amine-modified complementary DNA strands at 1 μM/OD550, then washed three times. A large excess of the MAL-dPEG4-NHS linker (Quanta Biodesign) was added at 30 μM/OD550 and incubated at room temperature for 1 hour, then washed three times to bring maleimide functional groups onto DNA scaffolds. Reduced antibodies with free thiols (FITC-IgG, Sigma) were conjugated to the maleimide groups using the above protocol.

To conjugate GFP to the functional groups presented by DNA-scaffolds, particles were hybridized with 3'thiol-modified complementary DNA strands at 1 μM/OD550 and decapped by TCEP with above protocol, then washed three times. The MAL-PEG4-NHS linker (Quanta Biodesign) was mixed with GFP at a 100-fold molar excess, incubated at 37°C for 1 hour, and then the excess was removed via size-exclusion chromatography. Freshly prepared particles and ~300 nM/OD550 linker-attached GFP were combined and reacted at room temperature for 1 hour, then washed three times.

Stability test in DNase and human serum

To test the stability of DNA scaffolds, PLGA microparticles were hybridized with fluorescently labeled complementary DNA strands, then loaded with human FITC-IgG (Sigma # SLBW7799) through surface step-by-step conjugation. Particles with and without IgG coverage were suspended in the enzyme reaction buffer (Promega #M6101) plus DNase (RQ1 RNase-free DNase, Promega #M6101) at 5 U per 1 OD550 × 50 μL and incubated at 37°C for 20 minutes. Then, a stop buffer was added (Promega #M6101), and the mixture was centrifuged at 10,000 x g for 10 minutes to collect the supernatant and pellet for the fluorescence-based analysis. Similarly, particles with and without IgG attachment, together with particles hybridized by GFP-DNA conjugates, were suspended in human serum

(bioWORLD #v13081400) and incubated for 1 hour at 37°C, then centrifuged to collect the supernatant and pellet for the fluorescence-based analysis.

To test the serum stability of particles, an NH_2-modified PLGA polymer (LG 50:50, Mw 30,000–40,000 Da) or an NH_2-modified PLA polymer (Akina #AI19, Mw 40,000 Da), dissolved in DMF, was reacted with a Cyanine3 (Cy3)-NHS ester (Lumiprobe #11020) at a 30-fold molar excess at room temperature for 1 hour, then the mixture repeatedly underwent 70%-ethanol precipitation and DMF re-dissolution to remove the unconjugated dye. 1 mg of the Cy3-labeled polymer was incorporated into the emulsion protocol for DNA-scaffolded (G strand) microparticles. Particles were suspended in human serum (bioWORLD #v13081400) and incubated at 37°C over 14 days, with aliquots being sampled for the fluorescence-based analysis as described above.

Cell lines and culture

K562 human myelogenous leukemia cells (ATCC #CCL-243) and A375 human malignant melanoma cells (ATCC #CRL-1619) were used in T cell killing experiments. K562 and A375 were lentivirally transduced to stably express human HER2, PD-L1, and GFP. All cell lines were FACS-sorted for expression of the transgenes. Murine pro-B cell line BA/F3 (DSMZ #ACC 300), T cell lymphoma line EL4 (DSMZ #ACC 831), and bone marrow line 32D (DSMZ #ACC 411) were used to test synthetic circuit activation in mouse cells. BA/F3 and 32D cell lines were cultured in RPMI 1640 (Thermo Fisher #11875085) with 10% fetal bovine serum (FBS, UCSF Cell Culture Facility), 10 ng/mL mouse IL-3 (Thermo Fisher #PMC0035), and Penicillin-Streptomycin (Sigma #P4333). The EL4 cell line was cultured in RPMI 1640 (Thermo Fisher #11875085) with 5% fetal bovine serum (FBS, UCSF Cell Culture Facility) and Penicillin-Streptomycin (Sigma #P4333). A murine macrophage cell line J77A4.1 (ATCC TIB-67) was used for particle uptake assay. K562 cells were cultured in Iscove's Modified Dulbecco's Medium (Corning #10–016-CV) with 10% fetal bovine serum (FBS, UCSF Cell Culture Facility) and gentamicin (UCSF Cell Culture Facility). A375, J77A4.1 cells, and Lenti-X 293T packaging cells (Clontech #11131D) were cultured in Dulbecco's Modified Eagle's Medium (Gibco #10569–010) with 10% FBS. All cell lines in this work were tested negative for mycoplasma contamination.

Macrophage uptake assay

The biotin-modified "self"-peptide (biotin-miniPEG-GNYTCEVTELTREGETIIELK[Lys(FITC)], LifeTein) was loaded onto streptavidin-tethered PLGA microparticles using the protocol described above. The streptavidin on the control particles without the "self-peptide" was labeled with NHS-fluorescein (ThermoFisher #46409) at 6 μM/OD550 for 1 hour at room temperature, then washed three times. The murine macrophage cell line J77A4.1 (ATCC) grown on glass-bottom chamber slides (Thermo Scientific #154526) was treated with lipopolysaccharides (Sigma #L4391) at 100 ng/mL overnight. The next day, "self"-peptide-loaded particles and control particles were added at 0.03 OD550 × 200 μL and incubated at 37°C for 1 hour. Cells were then washed three times with PBS to remove non-internalized particles, and then they were fixed using 4% paraformaldehyde (Electron Microscopy Sciences #15710) for 20 minutes. After three washes, cells were imaged using the spinning disk confocal fluorescence microscope

(Nikon Yokogawa CSU-22). Images were analyzed for cell fluorescence signals using ImageJ 2.0.0 software.

Primary human T cell isolation and culture

Blood was obtained from Blood Centers of the Pacific (San Francisco, CA) as approved by the University Institutional Review Board. Primary CD4+ and CD8+ T cells were isolated from anonymous donor blood samples after apheresis by negative selection (STEMCELL Technologies #15062 and #15063). T cells were cryopreserved in RPMI-1640 (Corning #10–040-CV) with 20% human AB serum (Valley Biomedical, #HP1022) and 10% DMSO. After thawing, T cells were cultured in human T cell medium consisting of X-VIVO 15 (Lonza #04–418Q), 5% Human AB serum, and 10 mM neutralized N-acetyl L-Cysteine (Sigma-Aldrich #A9165) supplemented with 30 units/mL IL-2 (NCI BRB Preclinical Repository) for all experiments.

Antibody staining and flow cytometry analysis

All antibody staining for flow cytometry was carried out in the wells of round-bottom 96-well tissue culture plates. The plates were centrifuged for 4 minutes at 400 x g, resulting in pelleting of the cells. The supernatant was removed, and the cells were resuspended in 50 μL PBS containing the fluorescent antibody of interest. Cells were stained after 25 minutes at 4°C in the dark. Stained cells were then washed twice with PBS and resuspended in fresh PBS for flow cytometry with a BD LSR II or a BD LSRFortessa. All flow cytometry data were collected using BD FACSDiva Software 8.0.1 and the analysis was performed in FlowJo software 10.7.1.

ICEp-mediated activation of human primary T cells for *ex vivo* activation

Anti-CD3/CD28-ICEp were synthesized using PLGA microparticles functionalized with anti-CD3 antibodies (Bio X Cell #BE0001–2, attached to 3'NH_2-5'Qusar670-modified compB) and anti-CD28 antibodies (Bio X Cell #BE0248, attached to 3'NH_2-5'FAM-modified compR) at varying ratios, including 1:5, 1:3, 1:1, 3:1 to 5:1, according to the method described above. After thawing and a 24-hour recovery in culture, 1.4×10^5 CD4+/CD8+ human primary T cells in 200 μL medium were added to ICEp at 0.11 OD550 (approximately 2.5 ICEp to 1 cell) or to CD3/CD28 Dynabeads at a 1:2.5 cell:bead ratio (Life Technologies #11131D) for 4 days. CD8+ T Cells were imaged through the spinning disk confocal microscope (Nikon Yokogawa CSU-22) 0, 1, 8 and 14 days after ICEp addition. Dynabeads were removed using the magnetic plate 5 days after the cells were stimulated, whereas ICEp were not removed. CD4+ and CD8+ T cell numbers were quantified using a cell counter (Countess II FL AMQAF1000, ThermoFisher) every other day from day 6 to day 14 after ICEp activation. Medium containing fresh IL-2 was supplemented to maintain the cell concentration between 0.5–1.5 million per mL. T cell differentiation (day 7) and exhaustion (day 14) phenotypes were studied by flow cytometry analysis using the following antibodies: anti-CCR7 (BD #561271, 1:20 dilution and Biolegend #353226, 1:200 dilution), anti-CD45RA (BD #562885, 1:100 dilution, and Biolegend #304150, 1:200 dilution), anti-CD45RO (BD #564291, 1:200 dilution), anti-CD62L (Biolegend #304830, 1:200 dilution), anti-CD27 (Biolegend #356424, 1:200 dilution), anti-CD95 (Biolegend #305644, 1:200 dilution), anti-LAG-3 (BD #565720, 1:25

dilution), anti-TIM-3 (BD #565558, 1:25 dilution), and anti-PD-1 (Biolegend #329936, 1:25 dilution).

The anti-IL-2 clone #5355 (ThermoFisher #MA523696) was biotinylated using NHS-PEG_4-biotin (Quanta Biodesign #10200) at a 30-fold molar excess. The mixture was incubated at 37°C for 1 hour, then purified via size exclusion chromatography (ThermoFisher #89882). Streptavidin-tethered PLGA microparticles were incubated with biotinylated anti-IL-2 at 20 nM/OD550 and IL-2 (NCI BRB Preclinical Repository) at 1.5 or 30 nM/OD550 at room temperature for 30 minutes and washed twice. IL-2 loaded ICEp were added to IL-2-free T cell medium to obtain a final particle concentration of 0.005 OD550, and ICEp-[3:1]-treated T cells were replenished with this medium to maintain the cell concentration at 0.5–1.5 million per mL. As a comparison to free IL-2 supplementation at 30 units/mL (0.54 ng/mL), ICEp from 30 nM/OD550 IL-2 incubation (yield 114.0 ng/mL per OD550, 0.57 ng/mL in the medium, Supplementary Fig. 6g) was equivalent to free IL-2, while ICEp from 1.5 nM/OD550 incubation (yield 9.8 ng/mL per OD550, 0.049 ng/mL in the medium, Supplementary Fig. 6g) was about 10-fold less than free IL-2 supplementation.

Transduction of synthetic circuit in human primary T cells and murine cell lines

For the transduction of human primary T cells, the binding domain of the LaG17 nanobody[20] was cloned into synNotch receptors with the Gal4 DNA-binding domain, VP64, as a synthetic transcription factor[20]. The response element plasmids were modified from the pHR'SIN:CSW vector with five copies of the Gal4 DNA binding domain, a HER2-CAR in the multiple cloning site downstream of the Gal4 response elements, and a PGK promoter that constitutively drives mCherry expression to easily identify transduced T cells[20]. All constructs were cloned via InFusion cloning (Takara Bio #638910). A pantropic VSV-G pseudotyped lentivirus was produced via transfection of Lenti-X 293T cells with a pHR'SIN:CSW transgene expression vector and viral packaging plasmids pCMVdR8.91 and pMD2.G using Fugene HD (Promega #E2312). Human primary T cells were thawed the same day and, after 24 hours in culture, were stimulated with Human T-Activator CD3/CD28 Dynabeads (Life Technologies #11131D) at a 1:2.5 cell-to-bead ratio. At 48 hours, the viral supernatant was harvested, and the primary T cells were exposed to the virus for 24 hours. At day 5 after T cell stimulation, Dynabeads were removed, and the T cells expanded until day 12 when they were rested and could be used in assays. T cells were sorted for assays with a BD FACSAria II on day 5 post-T cell stimulation.

For murine immune cell lines 32D, BA/F3, and EL4, a LaG17-synNotch receptor and response element vector were transduced using a lentivirus using the same protocol mentioned above. Differently, the response element vector plasmids were modified from the pHR'SIN:CSW vector with five copies of the Gal4 DNA binding domain target sequence 5' to a minimal CMV promoter driving BFP expression and PGK promoter driving mCherry expression. Medium containing the viral particles was collected from Lenti-X 293T cells, filtered through a 0.45 μm filter, and added to the immune cells for 24 hours. Sorted cells were expanded in their respective medium and cryopreserved for further experiments.

In vitro stimulation of synNotch T cells through ICEp

2.5×10^4 synNotch CD4+ or CD8+ primary T cells or murine cell lines were co-cultured with target cancer cells at a 1:1 ratio, with the addition of ICEp at 0.075 OD550 × 200 μL medium (100 μL T cell medium + 100 μL cancer cell medium) (unless otherwise specified). Dual antigen-positive (GFP and HER2) target cells (A375 and K562) and GFP-positive K562 cells were used as positive controls. After mixing, cells were centrifuged for 2 minutes at 300 x g to initiate interaction between the cells. After 24 hours, the co-culture from CD8+ T cells were stained with anti-CD69 antibody (BD #562884), analyzed by flow cytometry (BD LSR II), and imaged through the spinning disk confocal microscope (Nikon Yokogawa CSU-22). After 48 hours, cytokine concentration in the supernatant was measured by IL-2 ELISA (for CD4+ T cells, eBiosciences #BMS2221HS) and Interferon-γ (IFN-γ) ELISA (for CD8+ T cells, ThermoFisher #KHC4021).

To quantify target cell killing, 2.5×10^4 A375 cells were seeded on a flat-bottom 96-well tissue culture plate (Falcon #353072) and cultured for 8 hours, followed by the addition of 2.5×10^4 CD8+ T cells and ICEp at 0.075 OD550 × 200 μL final (unless otherwise specified). After 1–3 days, cells were gently washed with PBS twice and analyzed for cell viability using PrestoBlue Cell Viability Reagent (Invitrogen #A13262).

Particle localization and retention assay through IVIS imaging and tumor section

1 mg of a Cy3-labeled PLGA polymer, as described above, was incorporated into the emulsion protocol for DNA-scaffolded (G or B strand) PLGA microparticles. The surface of the particles was then hybridized with a 5'Quasar705 (Q705)-modified compG strand, 5'IR800CW-modified compG strand, or 5'Quasar670(Q670)-modified compB strand. Thereafter, human FITC-IgG (Sigma # SLBW7799) was loaded on the surface through step-by-step conjugation. NSG mice (Jackson Laboratory #005557, female, ~8–12-weeks old) were implanted with xenograft tumors: 5×10^6 K562 tumor cells subcutaneously either at the right flank or on both flanks. All mice were maintained in pathogen-free, ventilated cages with irradiated food and autoclaved water in housing conditions of humidity at 30–70%, temperature at 20–26°C and 12/12 dark/light cycle at the Laboratory Animal Resource Center (LARC) facilities at UCSF. All mice used throughout the work were handled under local, state and federal guidelines following an Institutional Animal Care and Use Committee (IACUC)-approved protocol at UCSF. Mice were monitored daily and euthanized by CO_2 asphyxiation and cervical dislocation prior to any signs of distress.

For IVIS animal imaging, 100 OD550 × 50 μL of particles with Q705-labeled DNA and FITC-IgG or 1 nmol free IR800CW carboxylate dye (Li-COR, #LIC-929–08972) were injected intratumorally 10 days after tumor implantation and imaged under the IVIS 100 preclinical imaging system (Xenogen #124262, with PerkinElmer Living Image Software 4.5.4) every 3–4 hours for the first 48 hours and every 8 hours for the next 5 days. Images are analyzed using PerkinElmer Living Image Software 4.5.4.

For the tumor section analysis, 100 OD550 × 50 μL of particles with Q670-labeled on DNA and FITC-IgG on surfaces and Cy3 in the core were injected intratumorally 10 days after tumor implantation. 6 hours, 2 days, 4 days, and 6 days after particle injection, mice were

euthanized, and the tumor and several organs, including the heart, lung, liver, kidney, and spleen were collected. These tissues were imaged under the IVIS imaging system. Tumors were fixed in 4% paraformaldehyde (Electron Microscopy Sciences #15710) overnight, then dehydrated in 30% sucrose (Sigma #S9378) for 1–2 days until the tumors sunk. Tumors were then snap-frozen in OCT (Tissue-Tek) to produce cryosections. Sections were imaged by the spinning disk confocal fluorescence microscope (Nikon Yokogawa CSU-22), and images were analyzed using the mean fluorescence intensity of the FITC and Q670 signal at particle locations identified by Cy3 signal using ImageJ 2.0.0 software.

Safety tests of DNA-scaffolded nano-/micro-particles

BALB/c mice (Jackson Laboratory #000651, female, ~7–9 weeks old) were intravenously injected with PLGA nanoparticles (~250 nm diameter) and microparticles (~1.5 μm diameter) with DNA scaffolds and mouse isotype IgG2b (BioXcell #BP0086) tethered through hybridization-mediated assembly. The injection dose was 20 OD550 × 100 μL for nanoparticles and 80 OD550 × 100 μL for microparticles, with an equivalent amount of surface DNA (~1.3 nmol) and isotype IgG (~20 μg). Blood was collected 2 days after particle injection and centrifuged at 14,000 x g for 5 minutes to collect the serum. 50 μL serum samples diluted in 200 μL PBS were sent to San Francisco General Hospital Clinical Laboratory for clinical chemistry tests. 50 μL serum samples diluted in 50 μL PBS were sent to Eve Technologies Inc. for cytokine/chemokine test (mouse cytokine/chemokine array 31-plex, MD31).

In vivo tumor targeting

NSG mice (Jackson Laboratory #005557, female, ~8–12 weeks old) were implanted with two identical xenograft tumors: 5×10^6 HER2+ K562 tumor cells subcutaneously on the left and right flank. Seven days after tumor implantation, human primary CD4+ (4×10^6) and CD8+ T cells (4×10^6) were injected intravenously into the tail vein of the mice. These T cells were either untransduced (control) or engineered with the anti-GFP synNotch Gal4VP64 receptor and the corresponding response elements regulating anti-HER2 4–1BB CAR expression. On the same day, ICEp-GFP particles were injected intratumorally on one side of the two flanks with 50 (or 10) OD550 × 50 μL per dose, leaving the other as the control. Three additional doses of ICEp were injected into the same tumor every 4 days or starting as soon as the tumor grew over 500 mm^3 in volume. Tumor size was monitored via caliper over 20 days after T cell injection. Mice were euthanized when any tumor reached 20 mm in diameter or became ulcerated.

Remaining tumors from the contralateral flank and early euthanized mice were collected and fixed in 4% paraformaldehyde (Electron Microscopy Sciences #15710) overnight, then dehydrated in 30% sucrose (Sigma #S9378) for 1–2 days until the tumors sunk. Tumors were then snap-frozen in OCT (Tissue-Tek) to produce cryosections. Sections were stained with anti-CD3 antibody (Biolegend #344811) in 1% BSA/PBS for 1 hour and washed three times, then imaged with the spinning disk confocal fluorescence microscope (Nikon Yokogawa CSU-22).

Statistical analysis

Statistical analyses were performed using GraphPad Prism 8.4.3 software. All values and error bars are mean ± s.d., except where indicated differently. Two-tailed *t* test, multiple *t* test, one-way ANOVA test, two-way ANOVA test, linear regression, lognormal fit, nonlinear fit by the Michaelis Menten model, Hill slope specific binding model, and fourth order polynomial model fit were performed and specified where appropriate.

Supplementary Material

Refer to Web version on PubMed Central for supplementary material.

Acknowledgements

We acknowledge the support by the National Institutes of Health Grant 1U54CA244438. We thank Z. Gartner for DNA synthesis, S. Habelitz for DLS analysis, C. Hayzelden for SEM imaging, B. Hann for IVIS imaging, K. Shokat for Tecan plate reader, and C. Zamecnik and A. Li for helpful discussion. X.H. was supported by a UCSF program for breakthrough biomedical research (PBBR) postdoc independent research grant and a Li foundation fellowship. J.Z.W. was supported by a Genentech Pre-Doctoral Fellowship. R.C. was supported by National Institute of General Medical Sciences (NIGMS) Medical Scientist Training Program #T32GM007618.

References

1. Riley RS, June CH, Langer R & Mitchell MJ Delivery technologies for cancer immunotherapy. Nat. Rev. Drug Discov 18, 175–196 (2019). [PubMed: 30622344]
2. Lim WA & June CH The Principles of Engineering Immune Cells to Treat Cancer. Cell 168, 724–740 (2017). [PubMed: 28187291]
3. Chen DS & Mellman I Oncology meets immunology: the cancer-immunity cycle. Immunity 39, 1–10 (2013). [PubMed: 23890059]
4. June CH & Sadelain M Chimeric Antigen Receptor Therapy. N. Engl. J. Med 379, 64–73 (2018). [PubMed: 29972754]
5. Gajewski TF, Schreiber H & Fu YX Innate and adaptive immune cells in the tumor microenvironment. Nat. Immunol 14, 1014–1022 (2013). [PubMed: 24048123]
6. Brudno JN & Kochenderfer JN Toxicities of chimeric antigen receptor T cells: recognition and management. Blood 127, 3321–3330 (2016). [PubMed: 27207799]
7. Riches JC et al. T cells from CLL patients exhibit features of T-cell exhaustion but retain capacity for cytokine production. Blood 121, 1612–1621 (2013). [PubMed: 23247726]
8. Gust J et al. Endothelial Activation and Blood-Brain Barrier Disruption in Neurotoxicity after Adoptive Immunotherapy with CD19 CAR-T Cells. Cancer Discov. 7, 1404–1419 (2017). [PubMed: 29025771]
9. Maus MV et al. T cells expressing chimeric antigen receptors can cause anaphylaxis in humans. Cancer Immunol. Res 1, 26–31 (2013).
10. Sagiv-Barfi I et al. Eradication of spontaneous malignancy by local immunotherapy. Sci. Transl. Med 10, eaan4488 (2018). [PubMed: 29386357]
11. Adachi K et al. IL-7 and CCL19 expression in CAR-T cells improves immune cell infiltration and CAR-T cell survival in the tumor. Nat. Biotechnol 36, 346–351 (2018). [PubMed: 29505028]
12. Wallace A et al. Transforming growth factor-beta receptor blockade augments the effectiveness of adoptive T-cell therapy of established solid cancers. Clin. Cancer Res 14, 3966–3974 (2008). [PubMed: 18559619]
13. Rafiq S et al. Targeted delivery of a PD-1-blocking scFv by CAR-T cells enhances anti-tumor efficacy in vivo. Nat. Biotechnol 36, 847–856 (2018). [PubMed: 30102295]
14. Tang H et al. Facilitating T Cell Infiltration in Tumor Microenvironment Overcomes Resistance to PD-L1 Blockade. Cancer Cell 29, 285–296 (2016). [PubMed: 26977880]

15. Shah NJ et al. An injectable bone marrow-like scaffold enhances T cell immunity after hematopoietic stem cell transplantation. Nat. Biotechnol 37, 293–302 (2019). [PubMed: 30742125]
16. Chen Q et al. In situ sprayed bioresponsive immunotherapeutic gel for post-surgical cancer treatment. Nat. Nanotechnol 14, 89–97 (2019). [PubMed: 30531990]
17. Ye Y et al. A melanin-mediated cancer immunotherapy patch. Sci. Immunol 2, eaan5692 (2017). [PubMed: 29127106]
18. Jiang W et al. Designing nanomedicine for immuno-oncology. Nat. Biomed. Eng 1, 0029 (2017).
19. Stephan SB et al. Biopolymer implants enhance the efficacy of adoptive T-cell therapy. Nat. Biotechnol 33, 97–101 (2015). [PubMed: 25503382]
20. Roybal KT et al. Precision Tumor Recognition by T Cells With Combinatorial Antigen-Sensing Circuits. Cell 164, 770–779 (2016). [PubMed: 26830879]
21. Brenner MJ, Cho JH, Wong NML & Wong WW Synthetic Biology: Immunotherapy by Design. Annu. Rev. Biomed. Eng 20, 95–118 (2018). [PubMed: 29345976]
22. Yu CS, Xi JC, Li M, An M & Liu HP Bioconjugate Strategies for the Induction of Antigen-Specific Tolerance in Autoimmune Diseases. Bioconjugate Chem. 29, 719–732 (2018).
23. Shao K et al. Nanoparticle-based immunotherapy for cancer. ACS Nano 9, 16–30 (2015). [PubMed: 25469470]
24. Li Y & Kurlander RJ Comparison of anti-CD3 and anti-CD28-coated beads with soluble anti-CD3 for expanding human T cells: differing impact on CD8 T cell phenotype and responsiveness to restimulation. J. Transl. Med 8, 104 (2010). [PubMed: 20977748]
25. Slifka MK & Amanna IJ Role of Multivalency and Antigenic Threshold in Generating Protective Antibody Responses. Front. Immunol 10, 956 (2019). [PubMed: 31118935]
26. Hartwell BL et al. Multivalent nanomaterials: learning from vaccines and progressing to antigen-specific immunotherapies. J. Pharm. Sci 104, 346–361 (2015). [PubMed: 25447598]
27. Shaw A et al. Binding to nanopatterned antigens is dominated by the spatial tolerance of antibodies. Nat. Nanotechnol 14, 398–398 (2019).
28. Shi BY et al. Challenges in DNA Delivery and Recent Advances in Multifunctional Polymeric DNA Delivery Systems. Biomacromolecules 18, 2231–2246 (2017). [PubMed: 28661127]
29. Sapsford KE et al. Functionalizing Nanoparticles with Biological Molecules: Developing Chemistries that Facilitate Nanotechnology. Chem. Rev 113, 1904–2074 (2013). [PubMed: 23432378]
30. Iyisan B & Landfester K Modular Approach for the Design of Smart Polymeric Nanocapsules. Macromol. Rapid Commun 40, e1800577 (2019). [PubMed: 30507023]
31. Huang X, Lai YF, Braun GB & Reich NO Modularized Gold Nanocarriers for TAT-Mediated Delivery of siRNA. Small 13, 1602473 (2017).
32. Cheung AS, Zhang DKY, Koshy ST & Mooney DJ Scaffolds that mimic antigen-presenting cells enable ex vivo expansion of primary T cells. Nat. Biotechnol 36, 160–169 (2018). [PubMed: 29334370]
33. Zhou J, Patel TR, Fu M, Bertram JP & Saltzman WM Octa-functional PLGA nanoparticles for targeted and efficient siRNA delivery to tumors. Biomaterials 33, 583–591 (2012). [PubMed: 22014944]
34. Douglas SM, Bachelet I & Church GM A logic-gated nanorobot for targeted transport of molecular payloads. Science 335, 831–834 (2012). [PubMed: 22344439]
35. Stephanopoulos N Hybrid Nanostructures from the Self-Assembly of Proteins and DNA. Chem 6, 364–405 (2020).
36. Hu Y & Niemeyer CM From DNA Nanotechnology to Material Systems Engineering. Adv. Mater, e1806294 (2019). [PubMed: 30767279]
37. Wang S et al. DNA-Functionalized Metal-Organic Framework Nanoparticles for Intracellular Delivery of Proteins. J. Am. Chem. Soc 141, 2215–2219 (2019). [PubMed: 30669839]
38. Peterson AM & Heemstra JM Controlling self-assembly of DNA-polymer conjugates for applications in imaging and drug delivery. Wiley Interdiscip. Rev.: Nanomed. Nanobiotechnol 7, 282–297 (2015). [PubMed: 25327363]

39. Wang ZG, Li N, Wang T & Ding B Surface-Guided Chemical Processes on Self-Assembled DNA Nanostructures. Langmuir 34, 14954–14962 (2018). [PubMed: 29884022]
40. Allahyari M & Mohit E Peptide/protein vaccine delivery system based on PLGA particles. Hum. Vaccines Immunother 12, 806–828 (2016).
41. Schmid D et al. T cell-targeting nanoparticles focus delivery of immunotherapy to improve antitumor immunity. Nat. Commun 8, 1747 (2017). [PubMed: 29170511]
42. Zamecnik CR, Lowe MM, Patterson DM, Rosenblum MD & Desai TA Injectable Polymeric Cytokine-Binding Nanowires Are Effective Tissue-Specific Immunomodulators. ACS Nano 11, 11433–11440 (2017). [PubMed: 29124929]
43. Blanco E, Shen H & Ferrari M Principles of nanoparticle design for overcoming biological barriers to drug delivery. Nat. Biotechnol 33, 941–951 (2015). [PubMed: 26348965]
44. Rodriguez PL et al. Minimal “Self” peptides that inhibit phagocytic clearance and enhance delivery of nanoparticles. Science 339, 971–975 (2013). [PubMed: 23430657]
45. Gattinoni L et al. A human memory T cell subset with stem cell-like properties. Nat. Med 17, 1290–1297 (2011). [PubMed: 21926977]
46. Arenas-Ramirez N et al. Improved cancer immunotherapy by a CD25-mimobody conferring selectivity to human interleukin-2. Sci. Transl. Med 8, 367ra166 (2016).
47. Tang L et al. Enhancing T cell therapy through TCR-signaling-responsive nanoparticle drug delivery. Nat. Biotechnol 36, 707–716 (2018). [PubMed: 29985479]
48. Singha S et al. Peptide-MHC-based nanomedicines for autoimmunity function as T-cell receptor microclustering devices. Nat. Nanotechnol 12, 701–710 (2017). [PubMed: 28436959]
49. Huang B et al. Active targeting of chemotherapy to disseminated tumors using nanoparticle-carrying T cells. Sci. Transl. Med 7, 291ra294 (2015).
50. Smith TT et al. In situ programming of leukaemia-specific T cells using synthetic DNA nanocarriers. Nat. Nanotechnol 12, 813–820 (2017). [PubMed: 28416815]
51. Kuai R, Ochyl LJ, Bahjat KS, Schwendeman A & Moon JJ Designer vaccine nanodiscs for personalized cancer immunotherapy. Nat. Mater 16, 489–496 (2017). [PubMed: 28024156]
52. Wang C, Ye Y, Hu Q, Bellotti A & Gu Z Tailoring Biomaterials for Cancer Immunotherapy: Emerging Trends and Future Outlook. Adv. Mater 29 (2017).

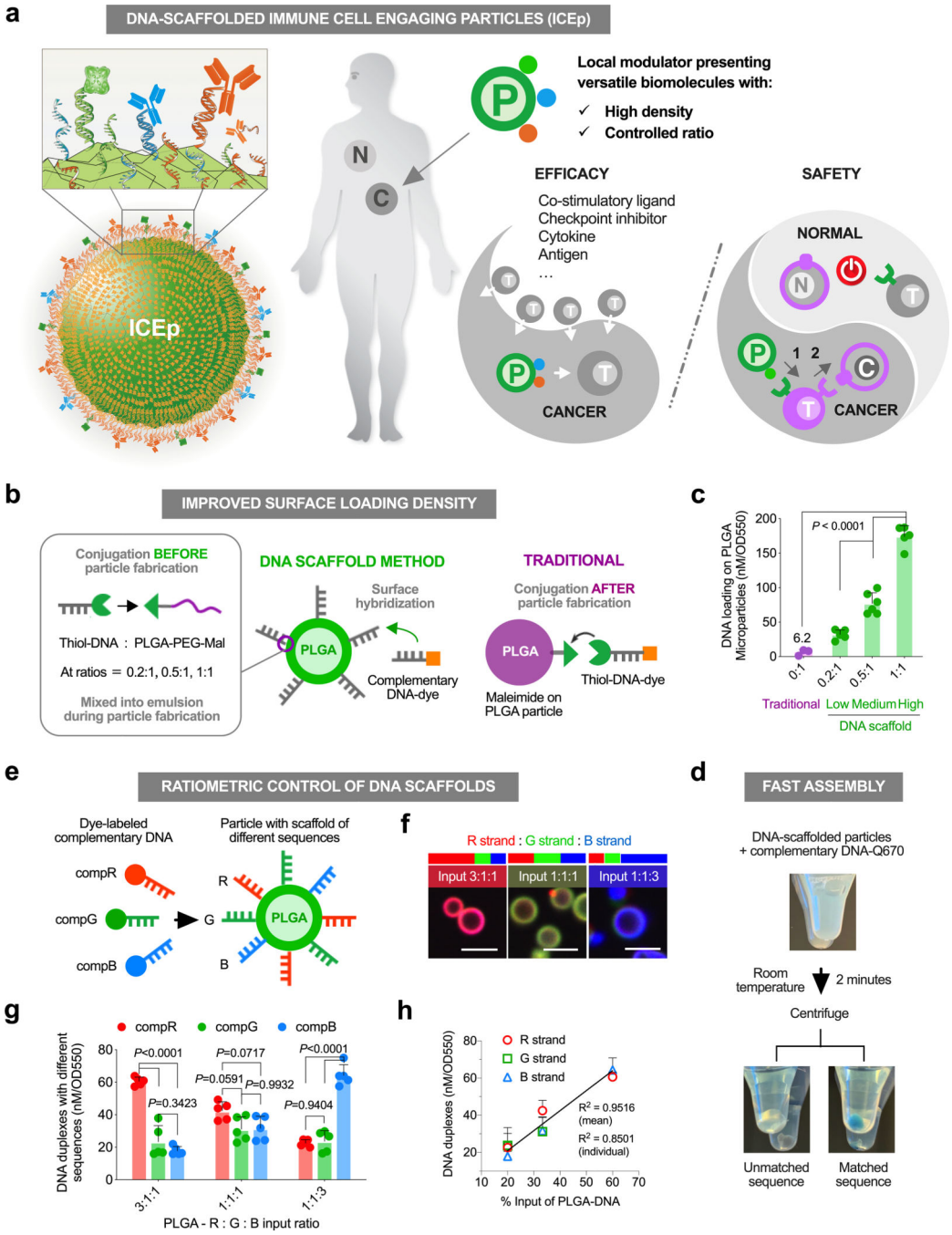

Figure 1.

Polymeric micro-/nanoparticles with surface DNA scaffolds for protein presentation allow versatile modulation of immune cell therapies. (**a**) Schematic of biodegradable polymeric particles presenting therapeutic proteins via surface DNA scaffolds with high density and ratiometric control, and their potential use as immune cell engaging particles (ICEp) for tumor microenvironment modulation and localized activation of natural or engineered immune cells. N: normal tissue, C: cancer cell, T: T cell, P: ICEp. (**b**) Schematic showing the construction of high and controlled densities of DNA scaffolds on polymeric particles

through a self-display of amphiphilic polymer-DNA molecules during the emulsion process, compared to the traditional surface conjugation method after particle fabrication. (**c**) Fluorescence-based analysis of hybridized, dye-labeled DNA duplexes on PLGA particles made from DNA-polymer conjugates of different coupling efficiencies versus dye-labeled DNA that was surface-conjugated to exposed functional groups on particles. Data are mean ± s.d. (n = 6 independent samples from 3 independent experiments), and *P* values were determined by one-way analysis of variance (ANOVA) and Tukey's tests. (**d**) Photos of PLGA microparticles in Eppendorf tubes after adding Quasar670 (Q670)-labeled complementary DNA to a matched or unmatched sequence for 2 minutes at room temperature. (**e**) Schematic displaying the control of DNA scaffolds with distinct sequences at intended ratios, which is confirmed by a corresponding dye-labeled complementary DNA (compDNA) hybridization assay. (**f**) Representative confocal microscopy images of PLGA microparticles with DNA scaffolds of different sequence compositions after hybridization with corresponding dye-labeled compDNA. The merged images of particles agreed with the theoretically integrated color at different input ratios. Scale bar, 5 μm. (**g**) Fluorescence-based analysis of DNA duplexes of different sequences on particles shown in (**f**). Data are mean ± s.d. (n = 5 independent samples from 2 independent experiments), and *P* values were determined by one-way analysis of variance (ANOVA) and Turkey's tests. (**h**) Correlation between hybridized duplexes of specific sequences on the surface and their corresponding DNA-polymer conjugate inputs shown in (**g**). Data are mean ± s.d. (n = 5 independent samples from 2 independent experiments), and the linear regression was created from individual replicates ($R^2 = 0.8501$) and the mean of each condition ($R^2 = 0.9516$).

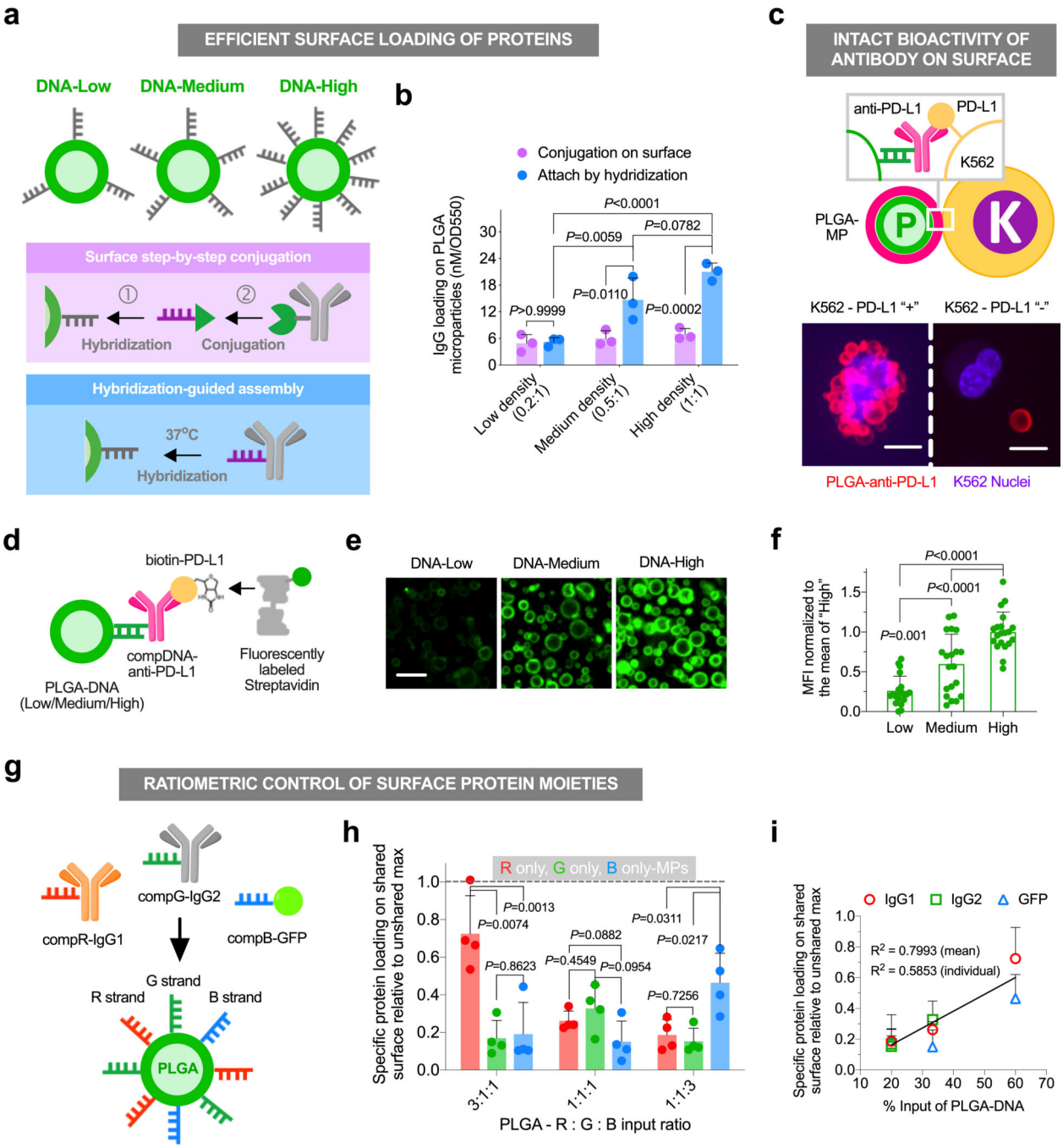

Figure 2.

DNA scaffolds enable efficient loading of multiple therapeutic proteins on particle surfaces at precisely tunable ratios. (**a**) Schematic of two strategies of protein loading on particles with DNA scaffolds: i) step-by-step conjugation through a bifunctional linker, and ii) hybridization-guided assembly of complementary DNA-protein conjugates. (**b**) Quantification of the FITC-labeled IgG loading density by the two strategies depicted in (**a**). Data are mean ± s.d. (n = 3 independent experiments), and *P* values were determined by one-way ANOVA and Turkey's tests. (**c**) Schematic of a PLGA microparticle loaded with an

anti-PD-L1 antibody binding to PD-L1-expressing K562 cells. Representative confocal microscopy images of co-incubated anti-PD-L1-tethered particles and PD-L1 +/− K562 cells (n = 3 biologically independent samples per group). Scale bar, 10 μm. (**d**) Schematic of a method that tests antigen-binding activity of surface-loaded antibodies. Biotinylated PD-L1 was used to bind active anti-PD-L1 on the particle surfaces, followed by the binding of fluorescently labeled streptavidin for detection. (**e**) Representative confocal microscope images of PLGA microparticles with different densities of DNA scaffolds that have been loaded with anti-PD-L1 antibodies followed by the assay described in (**d**) (n = 20 images from 4 independent experiments). Scale bar, 5 μm. (**f**) Quantification of the mean fluorescence intensity (MFI) of particles in images shown in (**e**). Data are mean ± s.d. (n = 20 images from 4 independent experiments), and *P* values were determined by one-way analysis of variance (ANOVA) and Tukey's tests. (**g**) Schematic showing how PLGA particles with DNA-scaffolds composed of distinct sequences enable the loading of specific ratios of therapeutic proteins. (**h**) Fluorescence-based analysis of the loading densities of three different proteins on the same surface guided by DNA scaffold compositions, relative to their individual, unshared maximums. Data are mean ± s.d. (n = 4 independent samples from 3 independent experiments), and *P* values were determined by one-way analysis of variance (ANOVA) and Tukey's tests. (**i**) Correlation between the specific protein loading on the surface and their corresponding DNA-polymer conjugate input during particle fabrication shown in (**e**). Data are mean ± s.d. (n = 3 independent experiments), and the linear regression was created from individual replicates (R^2 = 0.5853) and the mean of each condition (R^2 = 0.7993).

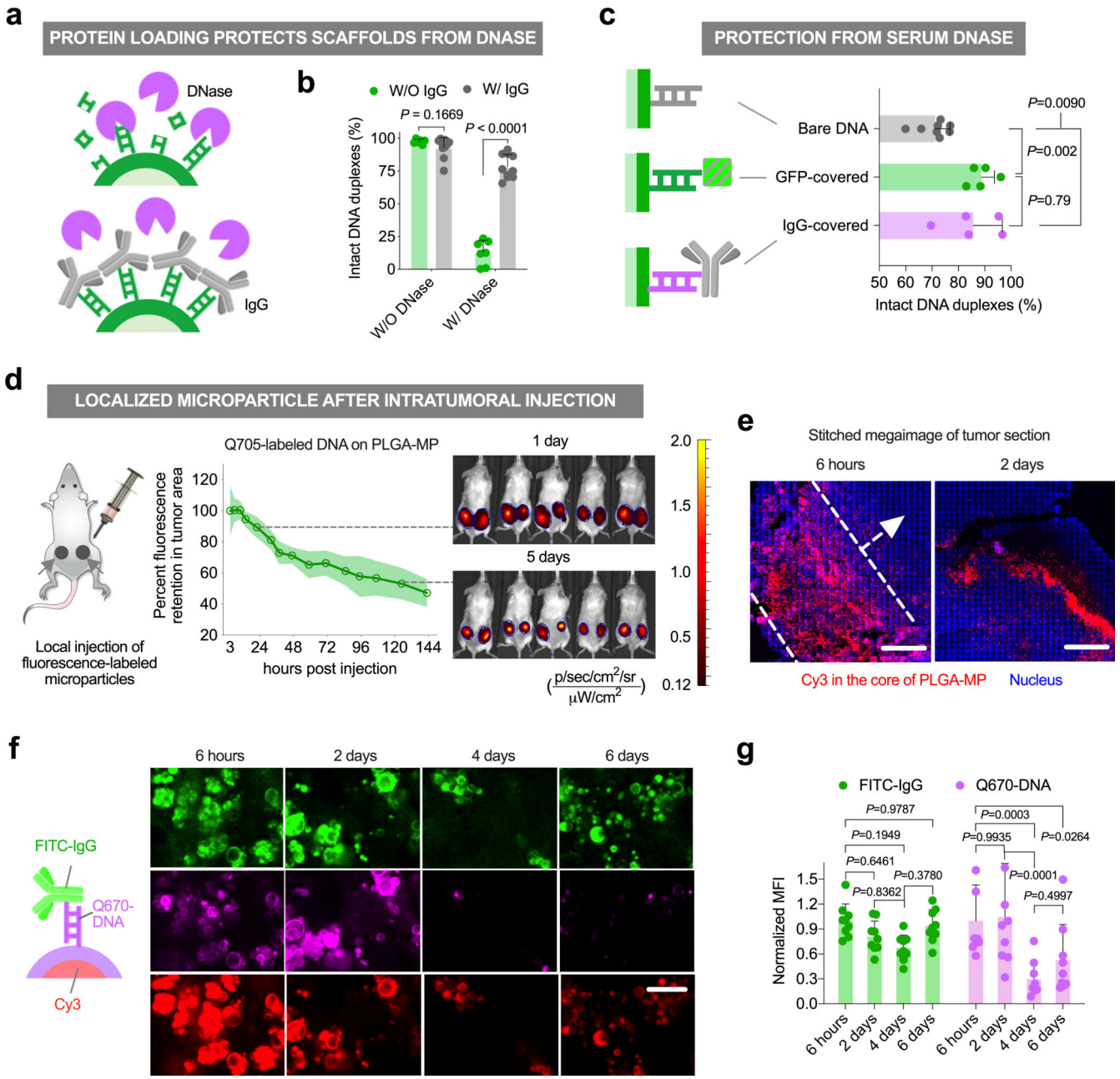

Figure 3.

Compatibility of DNA-scaffolded PLGA particles for *in vivo* applications. (**a**) Schematic showing that DNA scaffolds on the surface can be protected by protein attachment from DNase degradation. (**b**) Fluorescence-based analysis of intact DNA duplexes on PLGA microparticles after co-incubating with a large excess of DNase for 20 minutes. Data are mean ± s.d. (n = 3 independent experiments), and *P* values were determined by two-tailed paired *t* test. (**c**) Fluorescence-based analysis of intact DNA duplexes with different protein attachments on PLGA microparticles after incubation in human serum for 1 hour. Data are mean ± s.d. (n = 8 independent samples for “Bare DNA” and 5 independent samples for “GFP-covered” and “IgG-covered”, from 2 independent experiments) and *P* values were

determined by one-way ANOVA and Tukey's tests. (**d**) IVIS fluorescence imaging of NSG mice with subcutaneous K562 tumors that were injected with microparticles loaded with Quasar705 (Q705)-labeled compDNA and human IgG over 6 days (herein day 1 and 5), and quantification of signal intensity at the tumor area (right tumor with ICEp-PLGA) for the full set of IVIS images acquired over 6 days relative to 3 hours. Lines connect the means of relative signal intensity from n = 5 mice, and the shaded area denotes error band (± s.d.). (**e**) Representative stitched confocal microscope images of subcutaneous K562 tumor sections from NSG mice that were injected with Cy3 dye-conjugated (in the core) PLGA microparticles (with compDNA and human IgG on the surfaces) for 6 hours and 2 days (n = 3 mice). Scale bar, 1 mm. (**f**) Representative confocal microscope images of subcutaneous K562 tumor sections from NSG mice that were injected with PLGA microparticles with Cy3 dye conjugated in the core, Quasar670 (Q670)-labeled compDNA, and FITC-IgG on the surfaces at different time points, ranging from 6 hours to 6 days (n = 15 images from 3 mice at each time point). Scale bar, 20 μm. (**g**) Quantification of the mean fluorescence intensity of Q670-compDNA and FITC-IgG on microparticles in the tumor section images shown in (**f**). Data are mean ± s.d. (n = 9 images for 6 hours, 2 days, and 4 days and 6 images for 6 days, from 3 mice at each time point), and *P* values were determined by one-way ANOVA and Tukey's tests.

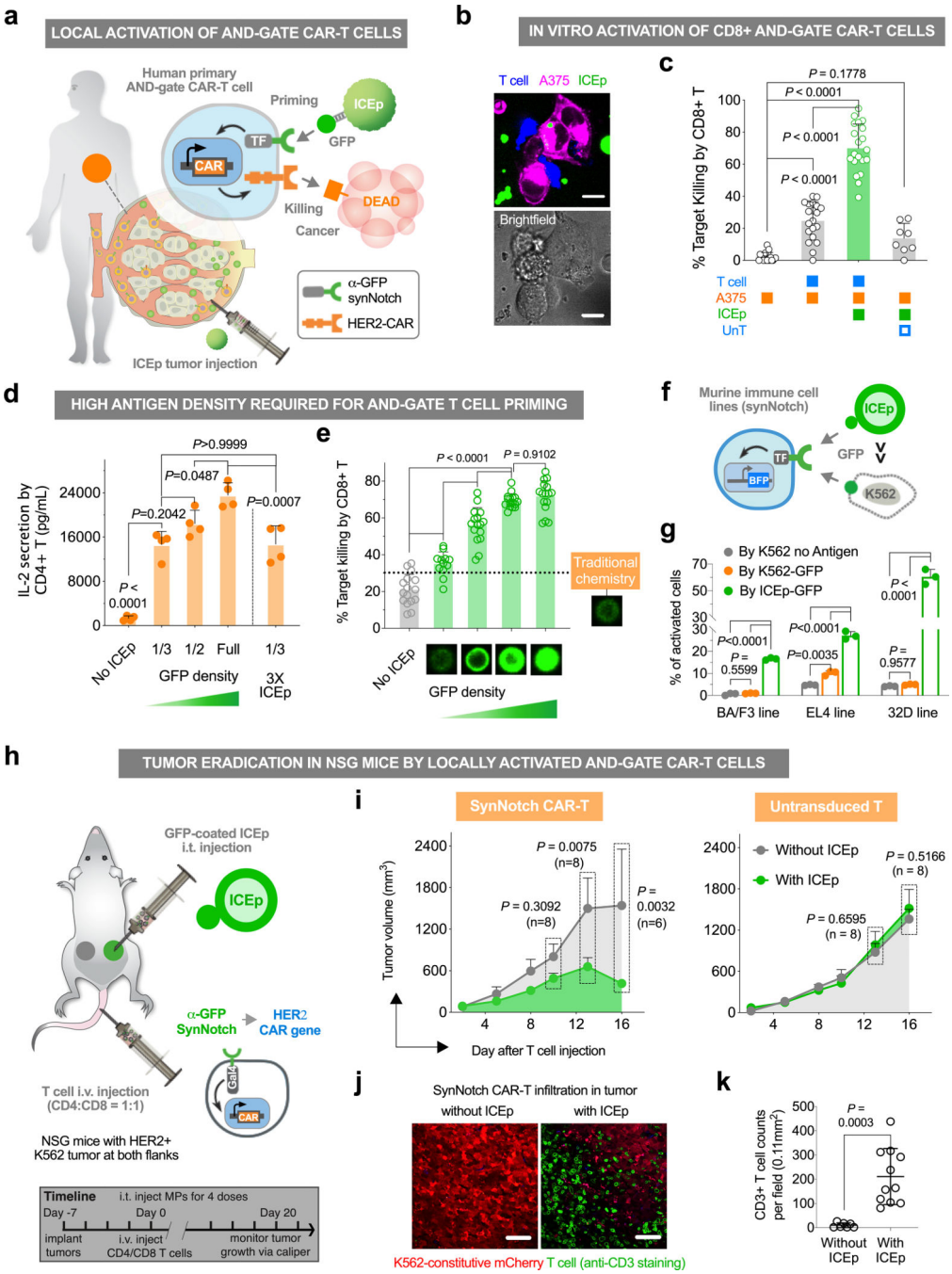

Figure 4.

Local activation of AND-gate CAR T cell for tumor killing by intratumoral injection of ICEp presenting a priming antigen. (**a**) Schematic showing the use of ICEp to present synthetic priming antigens (GFP) via intratumoral (i.t.) injection to locally prime synNotch-CAR AND-gate T cells to kill tumor cells. Primary human T cells were engineered with the anti-GFP synNotch and corresponding response elements regulating anti-HER2 4–1BB CAR expression. The synNotch-CAR T cells only express the CAR after sensing ICEp-presented GFP via synNotch binding, which should reduce ON-target OFF-tumor toxicity to

healthy organs also expressing the CAR antigen. (**b**) Representative confocal fluorescence microscopy image of the co-incubation of CD8+ synNotch CAR-T cells, ICEp-GFP, and HER2-overexpressing A375 cells after 24 hours (n = 2 independent experiments). Scale bar, 10 μm. (**c**) Target A375 cell killing test 48 hours after co-culture with ICEp-GFP and synNotch CAR-T cells. Data are mean ± s.d. (n = 6 independent experiment with 4 independent T cell donors), and *P* values were determined by one-way ANOVA and Tukey's tests. (**d**) IL-2 secretion by primary human CD4+ T cells after a 48-hour co-culture with HER2+ A375 target cells and ICEp with different GFP densities (e.g. 1/3, 1/2 and full). The total amount of antigen presented to T cells by ICEp particles with "Full" was equal to "1/3 × 3". Data are mean ± s.d. (n = 4 biologically independent samples from 2 independent experiments), and *P* values were determined by one-way ANOVA and Tukey's tests. (**e**) Killing efficacy of HER2+ A375 cells after a 48 hour co-culture with AND-gate T cells that were primed by ICEp with varying densities of GFP from DNA scaffolds compared to a traditional conjugation chemistry. Images are representative confocal fluorescence microscopic images of ICEp. Data are mean ± s.d. (n = 16 biological replicates from 4 independent experiments), and *P* values were determined by one-way ANOVA and Tukey's tests. (**f**) Schematic of ICEp-GFP versus GFP-expressing K562 cells activating murine immune cell lines that were engineered with anti-GFP synNotch and corresponding response elements regulating BFP expression. (**g**) The population of BFP+ murine immune cells that were activated by ICEp-GFP compared to GFP-expressing K562 cells and K562 cells without GFP antigen. Data are mean ± s.d. (n = 3 biological replicates), and *P* values were determined by one-way ANOVA and Tukey's tests. (**h**) Schematic of the NSG mice two tumor model for selected clearance by ICEp-primed synNotch CAR-T cell activation, while ICEp-GFP and engineered human primary CD4+/CD8+ T cells were administered through i.t. and intravenous (i.v.) injection, respectively. (**i**) Comparison between the volumes of the ICEp-injected tumor and the contralateral tumor of mice treated with engineered synNotch CAR-T cells (left graph) or untransduced T cells (right graph). Data are mean ± s.e.m. (n = 8 mice, and 2 mice met the euthanasia criteria at day 13–15), and *P* values were determined by two-tailed paired *t* test. (**j**) Representative images of fixed staining of tumor sections from one mouse that was sacrificed on an earlier date (Day 15) that met euthanasia criteria (n = 10 images). Scale bar, 50 μm. (**k**) Quantification of CD3+ T cell numbers in the stained tumor sections represented in (**j**). Data are mean ± s.d. (from n = 10 images), and *P* values were determined by two-tailed paired *t* test.

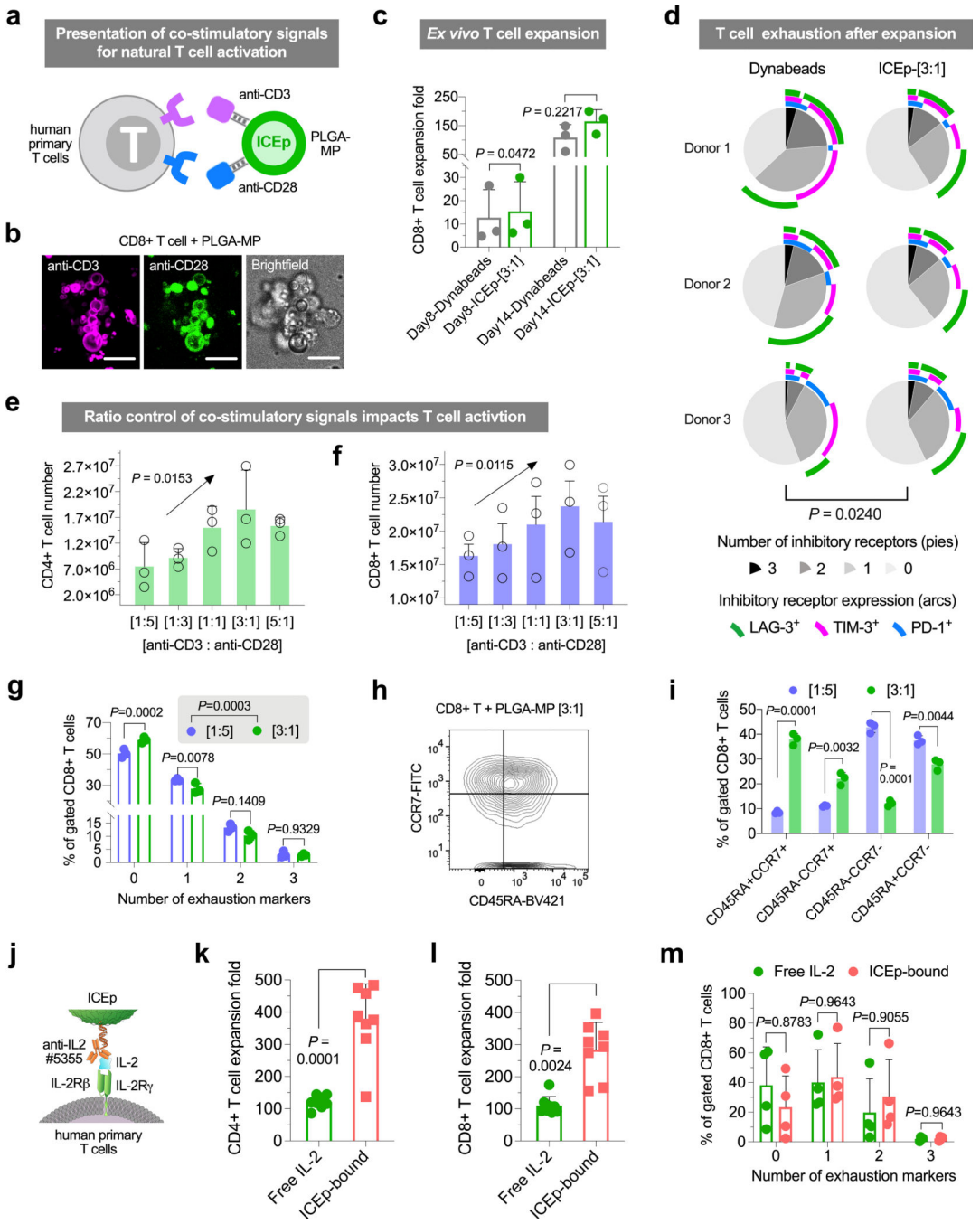

Figure 5.

ICEp, capable of versatile and precisely controlled modulatory signals, regulate T cell characteristics during *ex vivo* expansion. (**a**) Schematic of ICEp (PLGA microparticles with anti-CD3 and anti-CD28 antibodies controlled at specific ratios by DNA scaffolds, e.g. [1:5] to [5:1]) triggering human primary T cell activation and expansion. (**b**) Representative confocal microscopy images of human primary CD8+ T cell co-incubated with ICEp-[1:1] overnight, showing ICEp-induced cell clumps (n = 3 biologically independent samples). Scale bar, 10 μm. (**c**) Cell yield of human primary CD8+ T cells 8 and 14 days after

activation by ICEp-[3:1], compared to commercially available Dynabeads. Data are mean ± s.d., and *P* values were determined by two-tailed paired *t* test (n = 3 independent donors of 2 independent experiments). (**d**) Exhaustion marker analysis of CD8+ T cells after stimulation with ICEp-[3:1] or Dynabeads for 14 days. The *P* value was determined by nested one-way ANOVA analysis of cell population with 0 to 3 inhibitory receptors between ICEp-[3:1] and Dynabeads activation. (**e,f**) Cell yield of human primary CD4+ (**e**) and CD8+ (**f**) T cells 14 days after activation of 1.4×10^5 cells by ICEp with varying ratios of anti-CD3 to anti-CD28 ranging from [1:5] to [5:1]. Data are mean ± s.e.m. (n = 3 independent donors of 2 independent experiments), and *P* values were determined by one-way ANOVA test for linear trend. (**g**) The population of CD8+ T cells with 0 to 3 inhibitory receptors after being stimulated by ICEp-[1:5] or ICEp-[3:1] for 14 days. Data are mean ± s.d., and *P* values were determined by multiple *t* test for comparison of 0–3 subgroups and nested one-way ANOVA analysis for comparison between treatments of ICEp-[1:5] and ICEp-[3:1] (n = 3 independent donors of 2 independent experiments). (**h**) Representative two-dimensional dot plot of CCR7 and CD45RA expression on CD8+ T cells activated by ICEp-[3:1] for 7 days, and the gating strategy to analyze T cell differentiation phenotype. (**i**) CCR7 and CD45RA expression profile of CD8+ T cells stimulated by ICEp-[1:5] or ICEp-[3:1] for 7 days. Data are mean ± s.d. (n = 3 biological replicates from the same donor), and *P* values were determined by multiple *t* test with correction using the Holm-Sidak method. (**j**) Schematic of IL-2 presented on particles through its antibody (clone5355) that exposes the epitope for β and γ units of its receptor on T cells, thus promoting T cell proliferation. (**k,l**) Cell expansion profile of primary CD4+ (**k**) and CD8+ (**l**) T cells stimulated by ICEp-[3:1] for 14 days with ICEp-bound IL-2 or free IL-2 supplemented at an equivalent dose. Data are mean ± s.d. (n = 4 independent donors of 3 independent experiments), and *P* values were determined by two-tailed paired *t* test. (**m**) The population of CD4+ and CD8+ T cells with 0 to 3 inhibitory receptors stimulated by ICEp-[3:1] for 14 days with ICEp-bound IL-2 or free IL-2 supplemented at an equivalent dose. Data are mean ± s.d. (n = 4 independent donors of 3 independent experiments), and *P* values were determined by multiple *t* test with correction using the Holm-Sidak method.